M. G. Varzaneh, A. Rajaei, A. Jolfaei and M. R. Khosravi (2020) A High Step-Up Dual-Source Three-Phase Inverter Topology With Decoupled and Reliable Control Algorithm, *IEEE Transactions on Industry Applications,* vol. 56, no. 4, pp. 4501-4509

which has been published in final form at:
doi.org/10.1109/TIA.2019.2956715

A High Step-up Dual-Source Three Phase Inverter Topology with Decoupled and Reliable Control Algorithm

Majid Ghani Varzaneh
Shiraz University of Technology, Shiraz, Iran
m.ghani@sutech.ac.ir

Amirhossein Rajaei
Shiraz University of Technology, Shiraz, Iran
a.rajaei@sutech.ac.ir

Alireza Jolfaei
Department of Computing, Macquarie University, Australia
alireza.jolfaei@mq.edu.au

Mohammad R. Khosravi
Shiraz University of Technology, Shiraz, Iran
m.khosravi@sutech.ac.ir

Abstract- **In this paper, a new structure for dual-input single-output three phase inverters with a high voltage gain is presented. The proposed structure is based on the impedance source inverters, in which two independent input sources can share their power to supply a common load by replacing the high frequency transformers with some inductors. The proposed structure is also a voltage booster and is suitable for applications such as connecting to hybrid renewable energy systems. In the proposed structure, to improve the efficiency and to reduce the cost and structure weight, only one power conversion stage is used. In addition, the number of used semiconductors is lower than previous structures in the literature. As renewable energy sources such as wind and solar have the nature of intermittency, the supply of load in the systems which use them as inputs may be marred by some reliability problems. To this end, supplementary sources and also a fast control algorithm could be used to overcome the reliability problem. The proposed switching method controls the ratio of the power absorbed from the input sources and the dc-link voltage through the control of two independent variables. The reliability of the load supply is improved since the controller computes the parameters very fast. The experimental results on a 310 watt prototype confirm the theoretical analysis and the performance of the proposed inverter.**

Index Terms-- **Power Sharing, Hybrid Renewable Energy System, Dual-Source Inverter, Multi-Input Inverter, Z-source Inverter, Reliability, Decoupled Control Algorithm.**

I. INTRODUCTION

Power generation using renewable resources such as wind and solar energies has been increasing due to the continuous growth of energy demand and the destructive effect of fossil fuels to the planet. Due to the intermittency nature of renewable resources in supplying continuous power, supplemental power such as batteries or fuel cells are required [1]. Often when one of the input sources is a photovoltaic cell, for supplying the load continuously, another input is a fuel cell stack. In this situation, an structure, which gets two or more DC sources as the inputs to make an output, is required. Since AC loads have the highest demand, the structure produces AC voltage (or current) at the output.

The terminal voltage of renewable energy sources varies and is inherently too small. Therefore, to increase and control the output voltage, the use of voltage converters as interface between the sources and the consumer (or grid) is unavoidable [2, 3]. DC-DC converters, as a part of an interface between these sources and customers (or grid), should be used to increase these DC voltage values, and then an inverter is required to invert the DC voltage to AC [4].

Although by increasing the number of solar cells and connecting in series, the terminal voltage of the panel can be increased [5], this approach increases the partial shading effect which is undesirable [2, 6]. To overcome this problem, more complicated auxiliary circuits and algorithms are needed.

In hybrid energy systems based on photovoltaic and fuel cells, for converting DC to AC voltage, often four structures of power electronic infrastructure are used. These structures are illustrated in Fig. 1. The structures of Fig. 1 (a) and (c) are based on the use of single-input converters. These structures have often more active and passive elements than the structures of Fig. 1 (b) and (d), because in the first step of energy conversion, the number of single input converters and input sources are the same. Therefore, their efficiency are less and their cost, volume, and weight is higher. On the contrary, the control of the power absorbed from the various sources in the structures of Fig. 1 (a) and (c) is simpler than the other structures. The authors of [7-11] suggested that multi-input DC-DC converters can be used in the structure of Fig. 1 (b). In the structure of Fig. 1 (d), the control of the amount of power absorbed from each source and its degree of independence from the voltage and frequency of the load is very important. With respect to this structure, the topologies proposed in [12-17] are suitable for single-phase loads and the topologies proposed in [18-26] are suitable for three-phase loads. Although the control of shared power in the structure of Fig. 1 (d) is generally more difficult than the structure of Fig. 1 (b), we use a topology that belongs to the category of Fig. 1 (d) to reduce the cost, volume, and weight.

When the number of input sources is limited to three, the topology suggested in [18] is suitable for use. In this topology, none of the six switches of the inverter are common source, which makes the drive more complex. The topology introduced in [19] includes five more switches, and the topologies introduced in [21, 22, 25] include twelve more switches which generate a three-phase AC in the output using DC inputs. The topology in [19] has high reliability and it can still feed the load if one of the input sources gets disrupted. The topologies of [21, 22, 25] are useful for high power applications where no additional passive component is used.

As mentioned above, the output voltages of fuel cell stacks and photovoltaic cells are low, and therefore in most applications, the voltage level needs to be increases. A solutions to this problem is the use of impedance source

inverters [27]. In the various structures of the impedance source inverters proposed in [27], by making use of the shoot through concept, the value of dc-link voltage could be increased. This feature has also been used in the design of multi-input inverters by [20, 23, 24, 26]. The authors of [20] had major contribution in the presentation of multi-port inverters by using a combination of nine switches as introduced in [28] and a classical impedance source inverter as presented in [29]. The topology of [23] used a Trans-Z-source inverter presented in [30]. Similar to the topology presented in [18], the topology of [23] requires at least three input sources to have a three phase output.

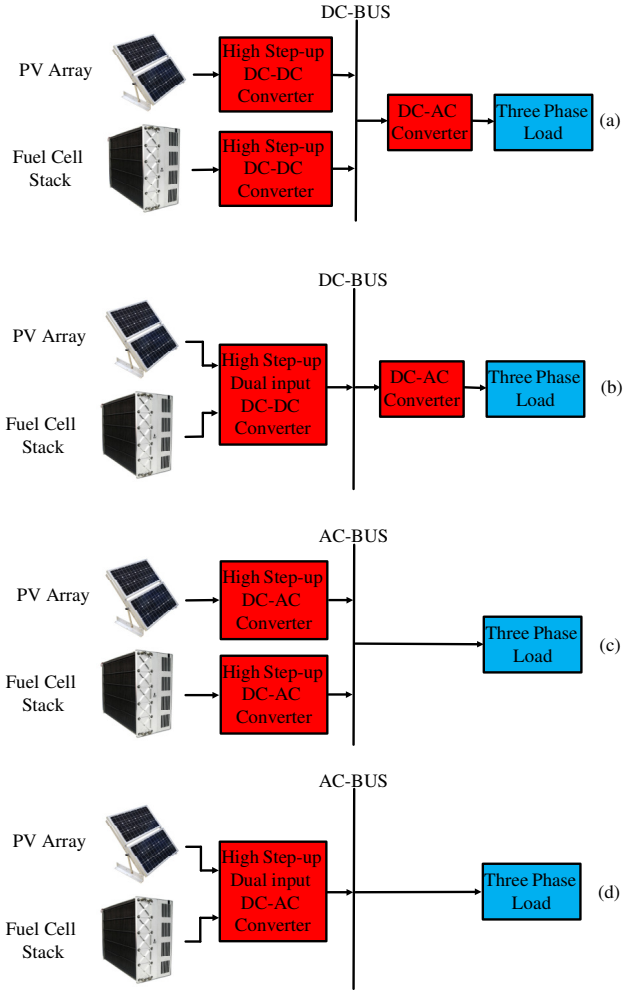

Fig. 1. All ways for connection hybrid PV-Fuel cell systems to AC loads: a) with single-input DC-DC converters, b) with dual-input DC-DC converters, c) with single-input DC-AC converters, d) with dual-input DC-AC converters.

Based on a classic Z-source inverter introduced in [29], the authors of [26] presented a method to make classic Z-source inverter to a multi-port inverter. However, in this method, there is not any control in the power generated by the sources and hence the controller cannot determine the variables to absorbed maximum rated power of the sources. Also, two or four sources used in this converter cannot have arbitrary voltage or current level.

In this paper, a multi-port structure is presented which contains two independent dc inputs and one three phase output. This structure only uses one extra switch. The design of this structure is based on the classic impedance source inverter [29]; therefore, this converter is a voltage booster. The converter is made from two classic impedance source inverters which connect to each other via some passive and active elements. These two impedance circuits can work with two different switching frequencies, simultaneously. The converter uses two high frequency three-winding transformers. The connections in this converter is such that the leakage inductances of the transformers do not cause problems such as voltage spike on the semiconductors.

In the proposed topology, there are two control variables, and through these two variables, trying to control the absorbed power ratio of two input sources and the value of dc-link voltage. One feature of the proposed topology is that the control of the absorbed power ratio of the input sources and the value of dc-link voltage is independent of each other. In other words, each one is changed by a control variable; therefore, the change in the value of dc-link voltage doesn't cause a change in the ratio of the power absorbed from the inputs and vice versa. The switching method used in this paper is *simple boost-SPWM* which introduced in[29].

In this paper, the proposed converter and all operation modes are described in section II. Section III are dedicated to extract the relations governing on the topology and analyze the power sharing study. The simulation and experimental results are described in Section IV. Section V concludes the paper.

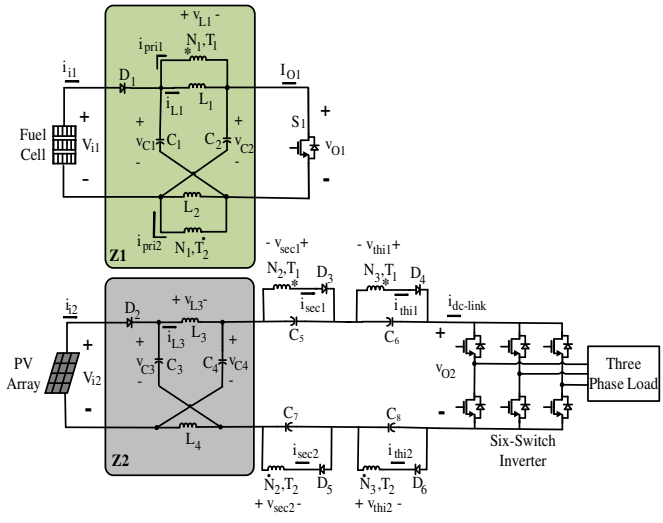

Fig. 2. Schematic diagram of the proposed dual-source three phase inverter

II. PROPOSED CONVERTER

Fig. 2 shows the proposed inverter, which is made up of two Z-source networks (*Z1* and *Z2*) supplied by two independent sources (V_{i1} and V_{i2}) with limited voltage level and a six-switch inverter connected to one load. In *Z1*, two

three-winding transformers (T_1 and T_2) are used instead of two inductors (compared to classic Z-Source introduced in [29]) which the magnetizing inductors of them, shown with L_1 and L_2, play the role of the inductors in classic Z-source inverter. In the proposed inverter, both *Z1* and *Z2* have two individual states, that is, shoot-through and non-shoot through states. When S_1 is turned on, *Z1* enters in shoot-through state and when two switches of one, two, or three legs of the six-switch inverter are turned on simultaneously, *Z2* enters in a shoot-through state; otherwise, there is a non-shoot through state. When *Z1* or *Z2* enters in shoot-through state, the inductors of them are charged and in non-shoot through state are discharged. Power sharing in this converter is performed via transformers, C_5, C_6, C_7, and C_8. The power flowed in the six-switch inverter and the load is divided between the two input sources. The control of power absorbed from the two input sources is performed by controlling the shoot-through duty cycles of *Z1* and *Z2*.

Z1 works according to the conditions pointed out in [29]. Accordingly, the relations that describe the average of the voltage values of *Z1* are as follows:

$$\frac{V_{C1}}{V_{i1}} = \frac{1-D_{st1}}{1-2D_{st1}} \quad (1)$$

$$\frac{V_{O1}}{V_{i1}} = \frac{1}{1-2D_{st1}} \quad (2)$$

where D_{st1} is the duty cycle of S_1. Other variables have been shown in Fig. 2. Following the circuit symmetry, $V_{C1} = V_{C2}$.

Assuming that the converter works in *CCM*, four states can be considered for the system as follows:

A) Both *Z1* and *Z2* are in shoot through state,

B) Z1 is in shoot through state and *Z2* is in non-shoot through state,

C) Z1 is in non-shoot through state and *Z2* is in shoot through state,

D) Both *Z1* and *Z2* are in non-shoot through state.

In the following, converter operation and the equivalent circuits during these states are discussed.

A) Z1 and Z2 are in shoot through state

D_1, D_2, D_4, and D_6 are off and D_3 and D_5 are on. L_1, L_2, L_3, L_4, C_5, and C_7 are charged through C_1, C_2, C_3, C_4, C_6, and C_8, respectively. Equivalent circuit and current paths are shown in Fig. 3 (a). In this figure, the current paths of *Z1* and *Z2* are shown with red and blue dashed lines, respectively.

B) Z1 is in shoot through state and Z2 is in non-shoot through state

In this mode, D_1, D_4, and D_6 are off and D_2, D_3, and D_5 are on. L_1, L_2, C_5, and C_7 are charged by C_1 and C_2. Also, L_3, L_4, C_6, and C_8 are discharged by the load. Also, C_3 and C_4 are charged by V_{i2}. Equivalent circuit and current paths are shown in Fig. 3(b).

C) Z1 is in non-shoot through state and Z2 is in shoot through state

In this mode, D_1, D_4, and D_6 are on and D_2, D_3, and D_5 are on. Because of volt-second law for L_1 and L_2, when *Z1* is in non-shoot through state, the voltage drops across L_1 and L_2 and consequently V_{sec1}, V_{sec2}, V_{thi1}, and V_{thi2} are negative. So D_3 and D_5 are off, D_4 and D_6 are on. In this mode, C_1, C_2, C_6, C_8, L_3, and L_4 are charged and other capacitors and inductors are discharged. The equivalent circuit and current paths are shown in Fig. 3 (c).

D) Z1 and Z2 are in non-shoot through state

Similar to mode *C*, in this mode, D_3 and D_5 are off. C_1, C_2, C_3, C_4, C_6, and C_8 are charged and the other capacitors are discharged. The equivalent circuit and current paths is shown in Fig. 3 (d).

The switching frequencies of *Z1* and *Z2* can be unequal; thus, the synchronization of *Z1* and *Z2* is not important. The switching method of the six-switch inverter shown in Fig. 2 is based on a simple boost pulse width modulation technique [29].

III. Steady State Relations and Power Sharing Analysis

According to the analysis, C_5, C_6, C_7, and C_8 are charged through *Z1* and are discharged by *Z2*. The charging of C_5 and C_7 is performed when *Z1* is in shoot through state and the charging of C_6 and C_8 is performed when *Z1* is in non-shoot through state. When *Z1* is in shoot through state (equivalent to *mode A* and *B*), V_{C1} and V_{C2} drop on the primary windings of the transformers and transfer to the secondary winding by turn ratio ($\frac{N_2}{N_1}$). At this situation, D_3 and D_5 are on and D_4 and D_6 are off, C_5 and C_7 are been charging and C_6 and C_8 are been discharging. Considering (1) and assuming ideal conditions of the converter:

$$\frac{V_{C5}}{V_{C1}} = \frac{V_{C7}}{V_{C1}} = \frac{N_2}{N_1} \quad (3)$$

Simplifying Equation (3) gives:

$$\frac{V_{C5}}{V_{i1}} = \frac{V_{C7}}{V_{i1}} = \frac{N_2}{N_1} \cdot \frac{1-D_{st1}}{1-2D_{st1}} \quad (4)$$

Again, when *Z1* is in non-shoot through state (equivalent to *mode C* and *D*), $V_{i1} - V_{C1}$ and $V_{i1} - V_{C2}$ drop on the primary windings of the transformers and transfer to the third winding by turn ratio $\frac{N_3}{N_1}$. At this situation, D_3 and D_5 are off and D_4 and D_6 are on, C_5 and C_7 are been discharging and C_6 and C_8 are been charging. By considering (1) and some simplifications:

$$\frac{V_{C6}}{V_{i1}} = \frac{V_{C8}}{V_{i1}} = \frac{N_3}{N_1} \cdot \frac{D_{st1}}{1-2D_{st1}} \quad (5)$$

Due to circuit symmetry, $V_{C3} = V_{C4}$. When *Z2* is in shoot through state, the voltage drops on L_3 is $V_{C3} + V_{C5} + V_{C6} + V_{C7} + V_{C8} = V_{C3} + 2V_{C5} + 2V_{C6}$, and for non-shoot through state the voltage is equal to $V_{i2} - V_{C4} = V_{i2} - V_{C3}$. Applying the volt-second law for L_3 yields:

$$(V_{C3} + 2V_{C5} + 2V_{C6}).D_{st2} + (V_{i2} - V_{C3}).(1 - D_{st2}) = 0 \quad (6)$$

where D_{st2} is the shoot through duty cycle of *Z2*. The substituting of (4) and (5) in (6) and simplification yields:

$$V_{C3} = \left(\frac{2D_{st2}}{1-2D_{st2}}\right) \cdot \left(\frac{N_2}{N_1} \cdot \frac{1-D_{st1}}{1-2D_{st1}} + \frac{N_3}{N_1} \cdot \frac{D_{st1}}{1-2D_{st1}}\right) \cdot V_{i1} + \left(\frac{1-D_{st2}}{1-2D_{st2}}\right) \cdot V_{i2} \quad (7)$$

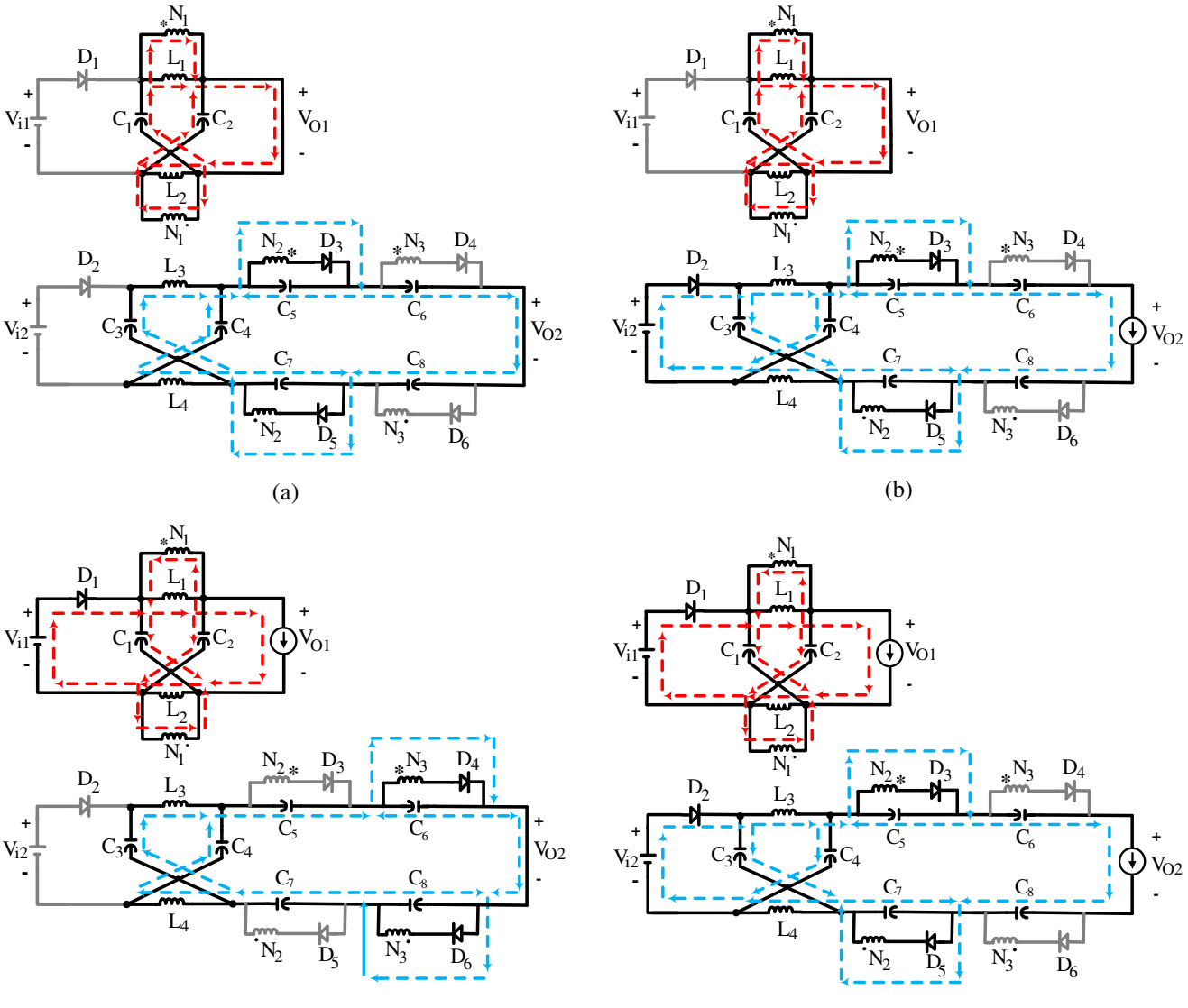

Fig. 3. The equivalent circuit of the system: a) for *mode A,* b) for *mode B,* c) for *mode C,* d) for *mode D.*

Similar analysis can be performed for dc-link voltage V_{O2}, when *Z2* is in non-shoot through state, is achieved as follow:

$$V_{O2} = 2\left(\frac{1}{1-2D_{st2}}\right)\cdot\left(\frac{N_2}{N_1}\cdot\frac{1-D_{st1}}{1-2D_{st1}}+\frac{N_3}{N_1}\cdot\frac{D_{st1}}{1-2D_{st1}}\right)\cdot V_{i1}+\left(\frac{1}{1-2D_{st2}}\right)\cdot V_{i2} \quad (8)$$

Equation (8) shows that the system is a boost converter, and this is a necessary feature for connecting to PV panels or fuel cell stacks. In the following, it is tried to compare the voltage gain with the voltage gains of the structures proposed in [20, 23].

In order to perform the comparison, it is assumed that $V_{i1} = V_{i2}$ and $\frac{N_3}{N_1} = \frac{N_2}{N_1} = n = 1$. The comparison is shown in Fig. 4. The figure shows the proposed converter has higher gain than the topology of [20, 23] for all values of D_{st1}. For example, for $D_{st1} = D_{st2} = 0.2$, the voltage gain of the proposed converter, [20], and [23] are 10.56, 1.67, and 1.43, respectively. If the value of n is increased or decreased, the gain of the proposed topology will be higher than the topologies of [20, 23].

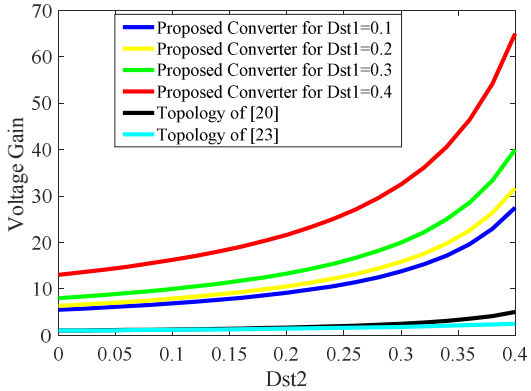

Fig. 4. The comparison of voltage gain for the converter and the topologies presented in [20, 23]

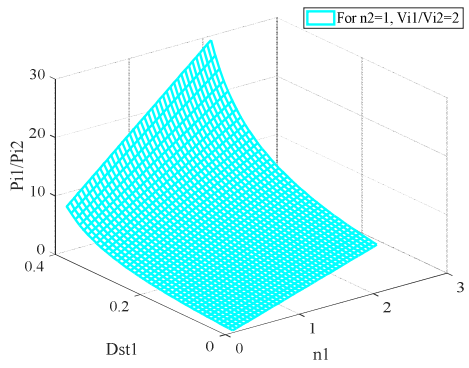

(a)

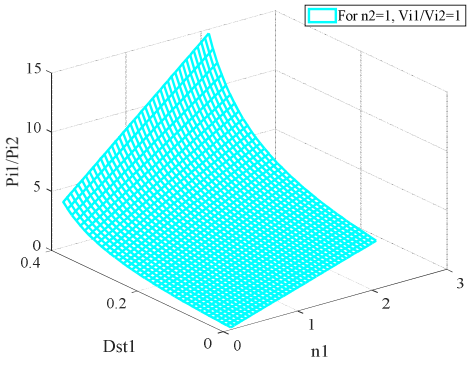

(b)

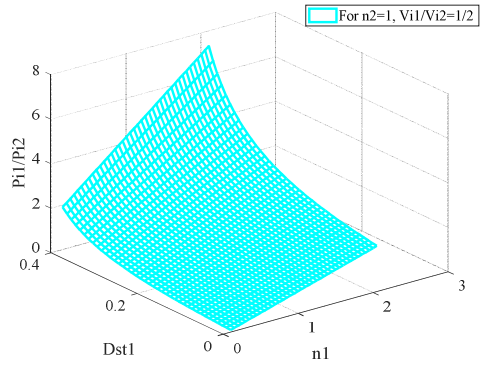

(c)

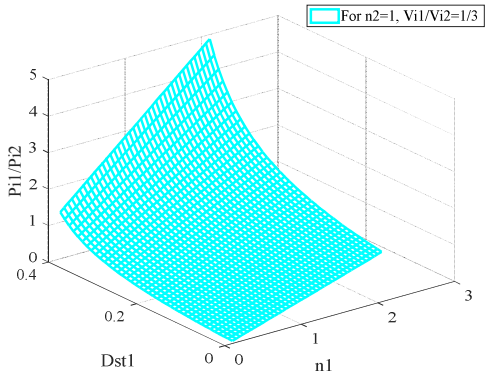

(d)

Fig. 5. $\frac{P_{i1}}{P_{i2}}$ with respect to D_{st1} and $n1$ for the different values of $\frac{V_{i1}}{V_{i2}}$. a) for $\frac{V_{i1}}{V_{i2}} = 2$, b) for $\frac{V_{i1}}{V_{i2}} = 1$, c) for $\frac{V_{i1}}{V_{i2}} = 1/2$, and d) for $\frac{V_{i1}}{V_{i2}} = 1/3$.

An important issue in multi-input converters is the ability to power sharing of the sources. For this purpose, here, the extracted power ratio from two input sources $\frac{P_{i1}}{P_{i2}}$ is selected as a controlling index. The index should be simple for implementation in the controller. Other variable which has to be controlled is V_{O2}. In other words, a equivalence device which consist of two equations, two dependent variables (V_{O2} and $\frac{P_{i1}}{P_{i2}}$), and two independent variable (D_{st1} and D_{st2}) has to be solved by the controller to supply the load at allowed values at any moment in time. Equation (8) describes the relation between V_{O2}, D_{st1}, and D_{st2}, so the equation which shows the relation between $\frac{P_{i1}}{P_{i2}}$, D_{st1}, and D_{st2} has to be extracted to complete the equivalence device. When *Z2* is in shoot through state,

$$I_{dc-link}^{st} = 2I_{L3} \tag{9}$$

where $I_{dc-link}^{st}$ is the average value of $i_{dc-link}$ in shoot-through time. When *Z2* is in non-shoot through state,

$$I_{dc-link}^{non\ st} = I_{Load} \tag{10}$$

where $I_{dc-link}^{non\ st}$ and I_{Load} are the average value of $i_{dc-link}$ and the load current in non-shoot through time, respectively. The average value of $i_{dc-link}$ in one switching period is obtained using both Equations (9) and (10) as follows:

$$I_{dc-link} = 2I_{L3} \cdot D_{st2} + I_{Load} \cdot (1 - D_{st2}) \tag{11}$$

Since $I_{dc-link} = I_{L3}$ and $I_{L3} = I_{i2}$, Equation (11) can be simplified as:

$$I_{i2} \cdot (1 - 2D_{st2}) = I_{Load} \cdot (1 - D_{st2}) \tag{12}$$

The active power absorbed by the load is

$$P_o = V_{O2} \cdot I_{Load} \cdot (1 - D_{st2}) \tag{13}$$

Substituting (12) in (13) yields:

$$P_o = V_{O2} \cdot I_{i2} \cdot (1 - 2D_{st2}) \tag{14}$$

The active power absorbed from input source 2 is:

$$P_{i2} = V_{i2} \cdot I_{i2} \tag{15}$$

Through Equations (14) and (15), we have:

$$P_{i2} = \frac{P_o \cdot V_{i2}}{V_{O2} \cdot (1 - 2D_{st2})} \tag{16}$$

The active power absorbed from the input source 1 is:

$$P_{i1} = P_o - P_{i2} \tag{17}$$

Substituting Equation (16) in Equation (17) simplifies Equation (17) as follows:

$$P_{i1} = P_o \cdot \left(1 - \frac{V_{i2}}{V_{O2} \cdot (1 - 2D_{st2})}\right) \tag{18}$$

The ratio of power absorbed from two inputs is achieved by dividing Equation (18) by Equation (16) as follows:

$$\frac{P_{i1}}{P_{i2}} = \frac{V_{O2} \cdot (1 - 2D_{st2}) - V_{i2}}{V_{i2}} \tag{19}$$

Substituting Equation (8) in Equation (19) results:

$$\frac{P_{i1}}{P_{i2}} = \frac{2\left(\frac{N_2}{N_1} \frac{1 - D_{st1}}{1 - 2D_{st1}} + \frac{N_3}{N_1} \frac{D_{st1}}{1 - 2D_{st1}}\right) \cdot V_{i1}}{V_{i2}} \tag{20}$$

Equation (20) shows that the control of power ratio depends on D_{st1} while it is independent of D_{st2}. This makes the controller simple. In the other hand, another variable which should be controlled is V_{O2}. Using Equations (8) and

(20), the relation for V_{O2} can be simplified as

$$V_{O2} = \left(\frac{P_{i1}}{P_{i2}} + 1\right) \cdot \left(\frac{1}{1-2D_{st2}}\right) \cdot V_{i2} \quad (21)$$

Equation (21) shows that for a specified value of $\frac{P_{i1}}{P_{i2}}$, V_{O2} can be controlled by D_{st2}.

Therefore, the value of $\frac{P_{i1}}{P_{i2}}$ and V_{O2} can be controlled by adjusting D_{st1} and D_{st2}, respectively. D_{st1} is determined by (20) and D_{st2} is determined by (21).

In Fig. 5, $\frac{P_{i1}}{P_{i2}}$ versus D_{st1} and $n1 = \frac{N_2}{N_1}$ is plotted for different values of $\frac{V_{i1}}{V_{i2}}$, when $n2 = \frac{N_3}{N_1} = 1$. The curves of this figure show if V_{i1}, V_{i2}, and $n1$ change, the controller can stabilize the value of $\frac{P_{i1}}{P_{i2}}$ in an acceptable range by changing D_{st1}. For drawing Fig. 5, the values of *n1* and *n2* is selected according to covering the area related to $n1 \geq n2$ and $n1 < n2$. Figs. 5 (a)-(d) show that with the increase of *n1* or D_{st1}, $\frac{P_{i1}}{P_{i2}}$ will increase. In Fig. 5, all curves have a similar trend.

IV. Simulation and Exprimental Results

To confirm the analyses, we used a 310 watt experimental prototype, as shown in Fig. 6. The switching frequencies of *Z1* and *Z2* are unequally selected to indicate the ability of the proposed converter to operate with two frequencies for two impedance networks, simultaneously. In our simulation and testing, the system has been evaluated using an open loop condition. We conducted our simulations using *Matlab Simulink*. In our testing, we used two large *LC* filters between the two inputs and the proposed converter, which makes the currents absorbed from the sources close to dc. Table I shows the values of system parameters. These parameters have been applied to simulation for simulating real condition and being possible comparison the simulation and experimental results. The experimental prototype, simulation and experimental results are shown in Figs. 6 to 10.

The test is performed in two steps; one is with a three-phase output filter and another is without the output filter. Fig. 10 (a) to (g) is extracted without filter and Fig. 10 (h) and (i) are extracted with the output filter. Fig. 8 (a) and (b) show that the amount of current absorbed from source 1 and 2 is 7.9 and 3.4 Ampere, respectively. The test results show that, as shown in Fig. 10 (a), the absorbed current from source 1 and 2 are 8 and 3.3 Ampere, respectively. Therefore, the input power absorbed from the input sources (without the output filter) is $V_{i1} \times I_{i1} + V_{i2} \times I_{i2} = 30 \times 8 + 30 \times 3.3 =$ 308.4Watt. Also, in the case of V_{O2}, it is observed that the value in the simulation (Fig. 9 (e)) and the test (Fig. 10 (c)) in non-shoot through state is 102 and 100 volt, respectively.

The operation of the system requires that the current of the transformers secondary windings in non-shoot through state and the transformers third windings in shoot through time be zero. The relation between the current of windings in shoot-through state is $i_{sec1} \times \frac{N_2}{N_1} = i_{pri1};\ i_{thi1} = 0$. Due to circuit symmetry, this relation also applies to i_{pri2}, i_{sec2}, and i_{thi2}. In non-shoot through state, the relation governing on the transformers windings is $i_{thi1} \times \frac{N_3}{N_1} = i_{pri1};\ i_{sec1} = 0$. Due to circuit symmetry, this relation is correct about i_{pri2}, i_{sec2}, and i_{thi2}. In Fig. 8 and Fig. 10, the windings current of the transformers are shown with counting the magnetizing currents (i_{L1} and i_{L2}). Therefore, for analyzing the relations said in this paragraph, it must be considered the effect of the magnetizing currents. For obtaining i_{L1}, in shoot through state, i_{sec1} must be multiplied by $\frac{N_2}{N_1}$ and then subtracted from primary current (shown in Fig. 8 (f) or Fig. 10 (b)). Again, in non-shoot through state, For obtaining i_{L1}, i_{thi1} must be multiplied by $\frac{N_3}{N_1}$ and then subtracted from the primary current. These analysis from simulation and experimental results and then comparison with each other verify that the prototype has good performance.

For other variables, such as inductors voltage and current, capacitors voltage, etc., it is observed that the simulation results (Fig. 8 andFig. 9) verify the experimental results shown in Fig. 10. The small variations between the simulation and experimental results are due to the lack of PCB modeling and parasitic elements of the prototype in the simulation.

For extracting the efficiency of the prototype in fundamental frequency (50 Hz), using the three-phase filter (2 mH inductors and 5 uF MKT capacitors) between the six-switch inverter and the load results: I_{i1}= 6.4 and I_{i2}=2 Ampere. In this case, the total active power absorbed from the input sources can be calculated from $V_{i1} \times I_{i1} + V_{i2} \times I_{i2} = 27 \times 6.4 + 28 \times 2 = 228.8$ Watt. The fundamental phase current flowed in the load is shown in Fig. 10 (i) which its amplitude is about 2 Ampere. The output power absorbed by the load in fundamental frequency is achieved from $3 \times R \times I^2_{rms-phase-50Hz} = 3 \times 22 \times (\frac{2}{\sqrt{2}})^2 = 199.18$ Watt. The efficiency, that is about % 87.1, is calculated by dividing the output power by the input power.

For analyzing power sharing ability of the proposed converter, referring to (21) (for $\frac{V_{i1}}{V_{i2}} = \frac{27}{28}, D_{st1} = 0.29,\ n1 = n2 = 1/2$) shows $\frac{P_{i1}}{P_{i2}} = 2.30$. Calculating the power ratio from experimental result (without using the output filter), which shown in Fig. 10 (a), shows $\frac{P_{i1}}{P_{i2}} = \frac{27 \times 8}{28 \times 3.3} = 2.33$. Again for this analysis, it can be said that because non-ideal model of the system hasn't been considered in section III, so small difference in the calculations in this topic is acceptable.

As can be seen in Fig. 9 (e)-(h) and Fig. 10 (c) and (d), the transformers leakage inductors can't make voltage spike on dc-link voltage and line-line voltages, so using the proposed converter in high power application doesn't require any attention about the protection of the switches and control the power loss.

Table. I. System Parameters

Parameters	Value
C_1, C_2, C_3, C_4, C_5, C_6, C_7, and C_8	1000 uF electrolytic capacitor paralleled with 1.5 uF polyester capacitor
L_1, L_2, L_3 and L_4	1200 uH
The resistance of L_3 and L_4	0.1 Ω
Primary windings of transformers	44 turn
Secondary windings of transformers	22 turn
Third windings of transformers	22 turn
Leakage inductance of the transformers primary winding	2 uH
Leakage inductance of the transformers secondary winding	1 uH
Leakage inductance of the transformers third winding	1 uH
Resistance of the transformers primary winding	0.2 Ω
Resistance of the transformers secondary winding	0.1 Ω
Resistance of the transformers third winding	0.1 Ω
D_1, D_2, D_3, D_4, D_5, and D_6	U1560 from Thinki Semiconductor company
Gate drive	ICL7667 from MAXIM company
Optocoupler	6N137 from VISHAY company
All power transistors (except S_1)	IRFP460 from VISHAY company
S_1	BUP314 from SIEMENS company
D_{st1}	0.29
D_{st2}	0.20
Modulation index	0.80
V_{i1}	27 Volt
V_{i2}	28 Volt
Switching frequency of Z1	15 kHz
Switching frequency of Z2	5 kHz
Fundamental frequency	50 Hz
Load (per phase)(star connection)	22 Ω
The controller of Z1 and Z2	PIC18F452 from Microchip company
Magnetic cores	Ferit EE6565 from Magnetic company

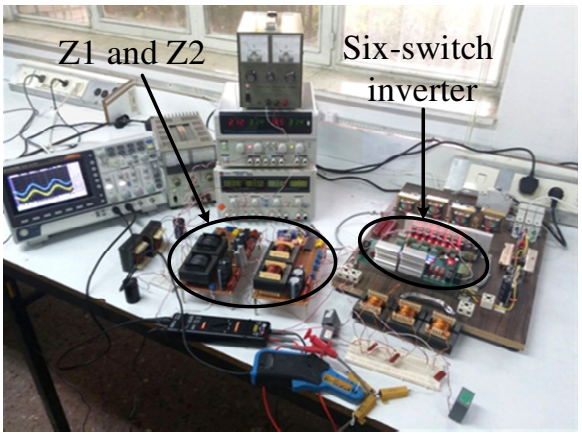

Fig. 6. The experimental setup

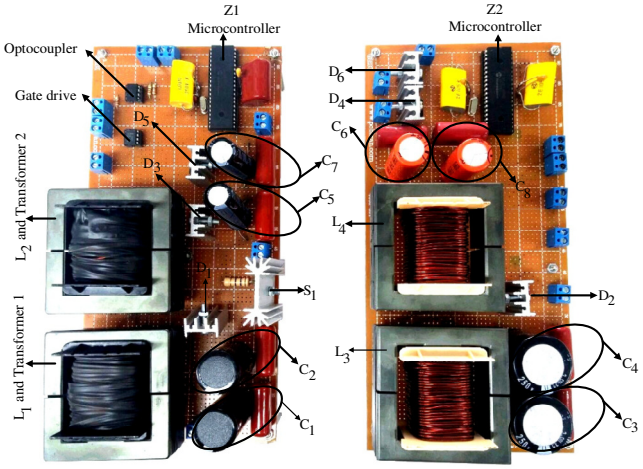

Fig. 7. *Z1* and *Z2* in the prototype

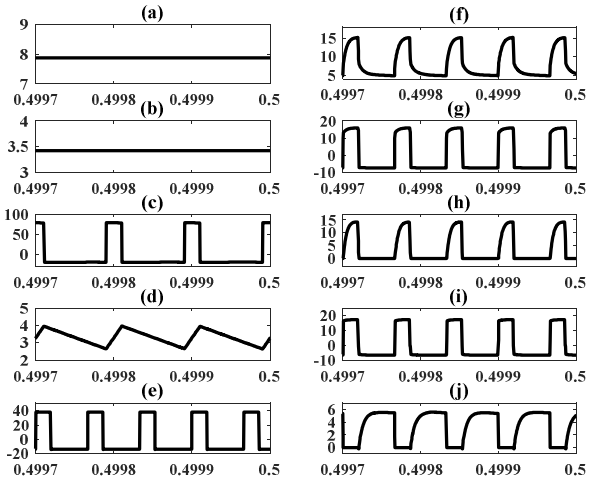

Fig. 8. Simulation results: a) I_{i1}, b) I_{i2}, c) v_{L3} or v_{L4}, d) i_{L3} or i_{L4}, e) v_{L1} or v_{L2}, f) primary current of the transformers (i_{pri1+} i_{L1} or i_{pri2+} i_{L2}), g) v_{sec1} or v_{sec2}, h) i_{sec1} or i_{sec2}, i) v_{thi1} or v_{thi2}, j) i_{thi1} or i_{thi2}. Horizontal axes are in seconds, and the vertical axes for current and voltage curve are amperes and volts, respectively.

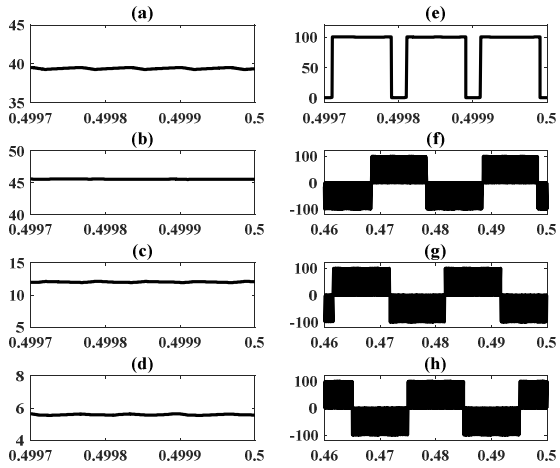

Fig. 9. Simulation results: a) V_{C1} or V_{C2}, b) V_{C3} or V_{C4}, c) V_{C5} or V_{C7}, d) V_{C6} or V_{C8} e) V_{O2}, f, g, h) Line-Line voltages. Horizontal and vertical axes are seconds and volts, respectively.

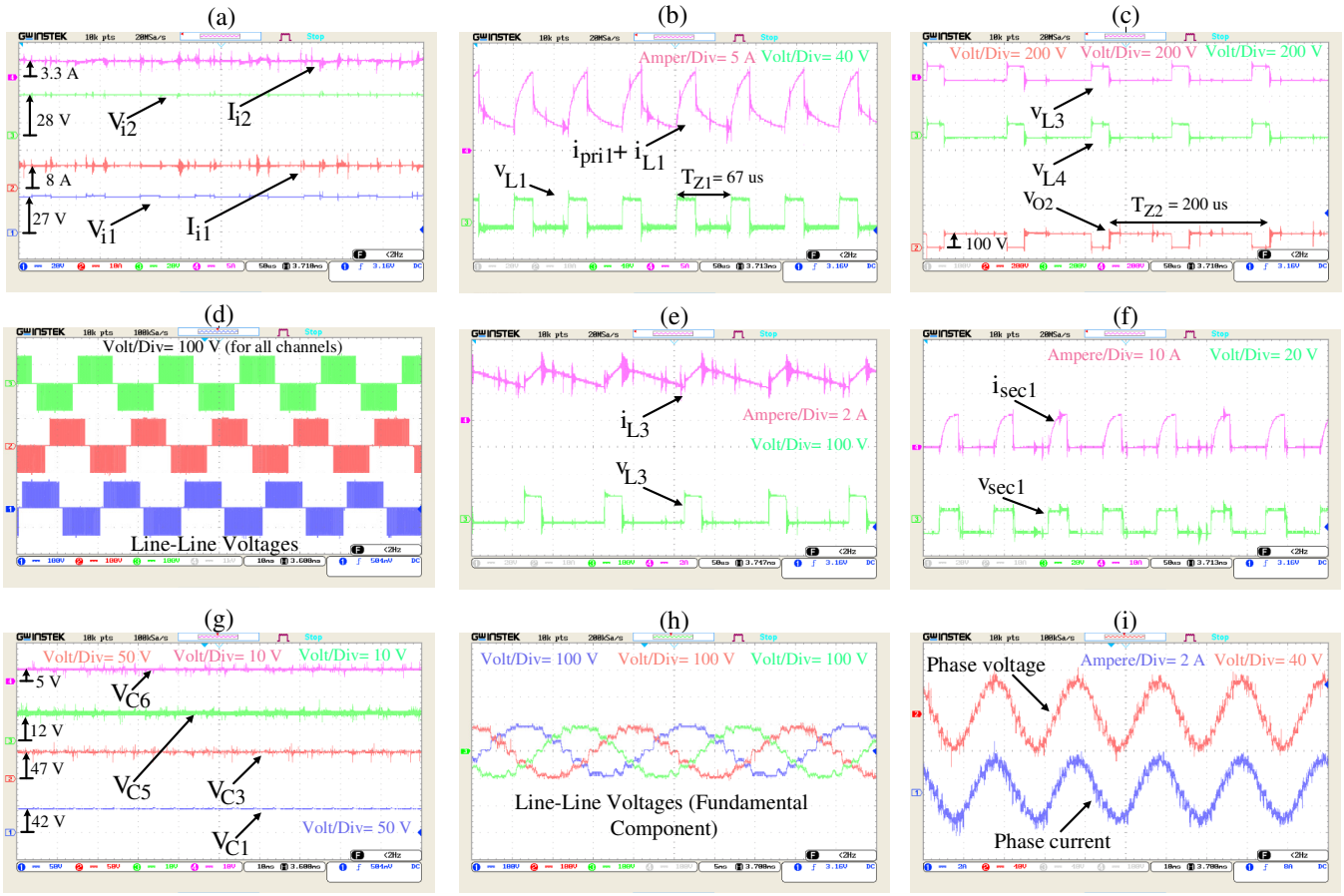

Fig. 10. Experimental results (Time/div: for (a), (b), (c), (e), and (f) is 50 μs, for (d), (g), and (i) is 10 ms, and for (h) is 5 ms.), (T_{Z1} and T_{Z2} are switching period of $Z1$ and $Z2$, respectively), (Volt/div and Ampere/div for each carve are added in the each part with specific colors)

V. Conclusion

In this paper, a new structure of dual-input single-output high gain inverters based on the impedance source inverters and three-winding transformers was presented. In this structure, the DC-AC transformation is performed in a single stage. This topology only requires an extra switch and a number of passive elements and diodes. Four modes have been defined and explained. This topology is a voltage booster converter that makes it possible to use it in renewable energy applications. Power sharing relationships have been extracted and explained. It has been proved that the dc-link voltage and the power ratio absorbed from the input sources can be controlled individually. The curves of absorbed power ratio show that the control of absorbed power ratio in different conditions for the transformers turn ratio and input voltages is possible. The simulation and experimental results verified performance and validity of the proposed inverter.

References

[1] S. K. Haghighian and S. H. Hosseini, "A novel multi-input DC/DC converter with a general power management strategy for grid connected hybrid PV/FC/battery system," in *Power Electronics, Drives Systems & Technologies Conference (PEDSTC), 2015 6th*, 2015, pp. 1-6: IEEE.

[2] T. Shimizu, K. Wada, and N. Nakamura, "Flyback-type single-phase utility interactive inverter with power pulsation decoupling on the DC input for an AC photovoltaic module system," *IEEE transactions on power electronics,* vol. 21, no. 5, pp. 1264-1272, 2006.

[3] Y.-P. Hsieh, J.-F. Chen, T.-J. Liang, and L.-S. Yang, "A novel high step-up DC–DC converter for a microgrid system," *IEEE Transactions on Power Electronics,* vol. 26, no. 4, pp. 1127-1136, 2011.

[4] L. Palma, M. H. Todorovic, and P. Enjeti, "A high gain transformer-less DC-DC converter for fuel-cell applications," in *Power Electronics Specialists Conference, 2005. PESC'05. IEEE 36th*, 2005, pp. 2514-2520: IEEE.

[5] L. Wang, C.-S. Lam, and M.-C. Wong, "Analysis, Control and Design of Hybrid Grid-Connected Inverter for Renewable Energy Generation with Power Quality Conditioning," *IEEE Transactions on Power Electronics,* 2017.

[6] H. Karimi, A. Yazdani, and R. Iravani, "Negative-sequence current injection for fast islanding detection of a distributed resource unit," *IEEE Transactions on Power Electronics,* vol. 23, no. 1, pp. 298-307, 2008.

[7] Y.-M. Chen, Y.-C. Liu, and S.-H. Lin, "Double-input PWM DC/DC converter for high-/low-voltage sources," *IEEE Transactions on Industrial Electronics,* vol. 53, no. 5, pp. 1538-1545, 2006.

[8] Y. Li, X. Ruan, D. Yang, F. Liu, and K. T. Chi, "Synthesis of multiple-input DC/DC converters," *IEEE Transactions on Power Electronics,* vol. 25, no. 9, pp. 2372-2385, 2010.

[9] H. Matsuo, W. Lin, F. Kurokawa, T. Shigemizu, and N. Watanabe, "Characteristics of the multiple-input DC-DC converter," *IEEE Transactions on Industrial Electronics,* vol. 51, no. 3, pp. 625-631, 2004.

[10] Q. Wang, J. Zhang, X. Ruan, and K. Jin, "Isolated single primary winding multiple-input converters," *IEEE Transactions on Power Electronics,* vol. 26, no. 12, pp. 3435-3442, 2011.

[11] A. Lavanya, J. D. Navamani, K. Vijayakumar, and R. Rakesh, "Multi-input DC-DC converter topologies-a review," in *Electrical, Electronics, and Optimization Techniques (ICEEOT), International Conference on*, 2016, pp. 2230-2233: IEEE.
[12] M. Azizi, M. Mohamadian, R. Beiranvand, and A. Rajaei, "Dual-input single-output DC-DC-AC converter," in *Power Electronics, Drive Systems and Technologies Conference (PEDSTC), 2013 4th*, 2013, pp. 315-320: IEEE.
[13] T. Mu, L. Zhu, H. Wu, and W. Jiang, "A semi-two-stage DC-AC power conversion system with improved efficiency based on a dual-input inverter," in *Energy Conversion Congress and Exposition (ECCE), 2016 IEEE*, 2016, pp. 1-6: IEEE.
[14] F. Yang, H. Ge, J. Yang, R. Dang, and H. Wu, "An asymmetrical multi-level dual-input dual-buck inverter for multi-source interface applications," in *Applied Power Electronics Conference and Exposition (APEC), 2017 IEEE*, 2017, pp. 2228-2233: IEEE.
[15] F. Yang, H. Ge, J. Yang, R. Dang, and H. Wu, "A Family of Dual-Buck Inverters With an Extended Low-Voltage DC-Input Port for Efficiency Improvement Based on Dual-Input Pulsating Voltage-Source Cells," *IEEE Transactions on Power Electronics,* vol. 33, no. 4, pp. 3115-3128, 2018.
[16] N. Zhang, D. Sutanto, and K. M. Muttaqi, "Design and control of a boost inverter based multi-input converter," in *Smart Grid Communications (SmartGridComm), 2016 IEEE International Conference on*, 2016, pp. 588-593: IEEE.
[17] L. Zhu, H. Wu, T. Mu, F. Yang, and X. Ma, "An asymmetrical three-level dual-input bidirectional DC/AC converter with improved conversion efficiency for vehicle-to-grid application," in *Applied Power Electronics Conference and Exposition (APEC), 2017 IEEE*, 2017, pp. 2062-2067: IEEE.
[18] M. Azizi, M. Mohamadian, and R. Beiranvand, "A new family of multi-input converters based on three switches leg," *IEEE Transactions on Industrial Electronics,* vol. 63, no. 11, pp. 6812-6822, 2016.
[19] E. Chemali and A. Emadi, "On the concept of a novel Reconfigurable Multi-Source Inverter," in *Transportation Electrification Conference and Expo (ITEC), 2017 IEEE*, 2017, pp. 707-713: IEEE.
[20] S. M. Dehghan, M. Mohamadian, A. Yazdian, and F. Ashrafzadeh, "A dual-input–dual-output Z-source inverter," *IEEE Transactions on power electronics,* vol. 25, no. 2, pp. 360-368, 2010.
[21] L. Dorn-Gomba, P. Magne, C. Barthelmebs, and A. Emadi, "On the concept of the multi-source inverter," in *Applied Power Electronics Conference and Exposition (APEC), 2016 IEEE*, 2016, pp. 453-459: IEEE.
[22] L. Dorn-Gomba, P. Magne, B. Danen, and A. Emadi, "On the Concept of the Multi-Source Inverter for Hybrid Electric Vehicle Powertrains," *IEEE Transactions on Power Electronics,* 2017.
[23] S. Jiang and F. Z. Peng, "Modular single-phase trans-Z-source inverter for multi-input renewable energy system," in *Applied Power Electronics Conference and Exposition (APEC), 2012 Twenty-Seventh Annual IEEE*, 2012, pp. 2107-2114: IEEE.
[24] J. Khajesalehi, K. Sheshyekani, M. Hamzeh, and E. Afjei, "High-performance hybrid photovoltaic-battery system based on quasi-Z-source inverter: application in microgrids," *IET Generation, Transmission & Distribution,* vol. 9, no. 10, pp. 895-902, 2015.
[25] C. Yan, S. Zou, and D. Xu, "Power control for dual-input DC/AC inverter," in *Power Electronics for Distributed Generation Systems (PEDG), 2015 IEEE 6th International Symposium on*, 2015, pp. 1-8: IEEE.
[26] D. Li, F. Gao, P. C. Loh, M. Zhu, and F. Blaabjerg, "Hybrid-source impedance networks: Layouts and generalized cascading concepts," *IEEE Transactions on power electronics,* vol. 26, no. 7, pp. 2028-2040, 2011.
[27] O. Ellabban and H. Abu-Rub, "Z-source inverter: Topology improvements review," *IEEE Industrial Electronics Magazine,* vol. 10, no. 1, pp. 6-24, 2016.
[28] C. Liu, B. Wu, N. R. Zargari, D. Xu, and J. Wang, "A novel three-phase three-leg ac/ac converter using nine IGBTs," *IEEE Transactions on Power Electronics,* vol. 24, no. 5, pp. 1151-1160, 2009.
[29] F. Z. Peng, "Z-source inverter," *IEEE Transactions on industry applications,* vol. 39, no. 2, pp. 504-510, 2003.
[30] W. Qian, F. Z. Peng, and H. Cha, "Trans-Z-source inverters," *IEEE transactions on power electronics,* vol. 26, no. 12, pp. 3453-3463, 2011.